Appl. Math. Mech. -Engl. Ed., **39**(12), 1769–1788 (2018)

Applied Mathematics and Mechanics (English Edition)

https://doi.org/10.1007/s10483-018-2400-9

Travel time prediction with viscoelastic traffic model*

Yongliang ZHANG[1], M. N. SMIRNOVA[2], A. I. BOGDANOVA[2], Zuojin ZHU[1,2], N. N. SMIRNOV[2,3,†]

1. Faculty of Engineering Science, University of Science and Technology of China, Hefei 230026, China;
2. Faculty of Mechanics and Mathematics, Moscow M. V. Lomonosov State University, Moscow 119992, Russia;
3. Scientific Research Institute for System Analysis, Russian Academy of Sciences, Moscow 117312, Russia

(Received May 2, 2018 / Revised Aug. 10, 2018)

Abstract Travel time through a ring road with a total length of 80 km has been predicted by a viscoelastic traffic model (VEM), which is developed in analogous to the non-Newtonian fluid flow. The VEM expresses a traffic pressure for the unfree flow case by space headway, ensuring that the pressure can be determined by the assumption that the relevant second critical sound speed is exactly equal to the disturbance propagation speed determined by the free flow speed and the braking distance measured by the average vehicular length. The VEM assumes that the sound speed for the free flow case depends on the traffic density in some specific aspects, which ensures that it is exactly identical to the free flow speed on an empty road. To make a comparison, the open Navier-Stokes type model developed by Zhang (ZHANG, H. M. Driver memory, traffic viscosity and a viscous vehicular traffic flow model. *Transp. Res. Part B*, **37**, 27–41 (2003)) is adopted to predict the travel time through the ring road for providing the counterpart results. When the traffic free flow speed is 80 km/h, the braking distance is supposed to be 45 m, with the jam density uniquely determined by the average length of vehicles $l \approx 5.8$ m. To avoid possible singular points in travel time prediction, a distinguishing period for time averaging is pre-assigned to be 7.5 minutes. It is found that the travel time increases monotonically with the initial traffic density on the ring road. Without ramp effects, for the ring road with the initial density less than the second critical density, the travel time can be simply predicted by using the equilibrium speed. However, this simpler approach is unavailable for scenarios over the second critical.

Key words travel time, viscoelastic modeling, distinguishing period for time averaging, spatial-temporal pattern, traffic jam

Chinese Library Classification O368
2010 Mathematics Subject Classification 35Q80

* Citation: ZHANG, Y. L., SMIRNOVA, M. N., BOGDANOVA, A. I., ZHU, Z. J., and SMIRNOV, N. N. Travel time prediction with viscoelastic traffic model. *Applied Mathematics and Mechanics* (*English Edition*), **39**(12), 1769–1788 (2018) https://doi.org/10.1007/s10483-018-2400-9

† Corresponding author, E-mail: wonrims@inbox.ru

Project supported by the Russian Foundation for Basic Research (No. 18-07-00518) and the National Natural Science Foundation of China (No. 10972212)

Nomenclature

$\boldsymbol{A}$,	Jacobian matrix;
B,	parameter used in Eq. (3);
B_0,	parameter defined by Eq. (9);
B_1,	$= 2u_x$;
B_*,	parameter defined by Eq. (7);
c,	traffic sound speed (m/s);
c_0,	sound speed at critical density ρ_{c2} (m/s);
c_τ,	speed depending on v_f and x_{br};
E_2,	parameter defined by Eq. (22);
$\boldsymbol{F}$,	$= (q, q^2/\rho + p)^T$, flux vector;
$\widehat{\boldsymbol{F}}_{i+1/2}$,	numerical flux at $x_{i+1/2}$;
G,	modulus of fluid elasticity used in Eq. (1);
K,	model parameter used in Eq. (4);
l,	average length of vehicles;
l_0,	length scale (m);
n,	time level;
p,	traffic pressure ($\rho_m v_f^2$);
q,	$= \rho u$, traffic flow rate (veh/s), where veh means vehiles;
q_e,	$= \rho u_e$, equilibrium traffic flow rate (veh/s);
R,	defined by Eq. (13);
R_1,	$= R + c^2\rho_x$;
t,	time (s);
t_0,	time scale (s);
t_{end},	time of simulation ended (s);
T_{tav},	mean travel time (s);
T_t',	root mean square (rms) of travel time (s);
$\boldsymbol{U}$,	$= (\rho, q)$, solution vector;
u,	traffic speed (m/s);
u_e,	equilibrium traffic speed (m/s);
u_{c2},	second critical speed (m/s);
v_0,	speed scale (m/s);
v_f,	free flow speed (m/s);
x,	coordinate (m);
X_{br},	braking distance of vehicles (m);
α,	$= l\rho_m$, parameter used to describe traffic pressure and sound speed;
β_0,	parameter used to define traffic pressure;
β,	$= \nu/2\tau_0 c_0^2$;
Δt,	time step (s);
Δx,	mesh length (m);
Δ_0,	preassigned distinguishing period (s);
λ_k,	eigenvalues of Eq. (14);
Λ,	$= c_\tau/u_{c2}$;
ρ,	traffic density (kg/m^3);
ρ_*,	first critical density (veh/km);
ρ_s,	saturation density (veh/km);
ρ_m,	traffic jam density (veh/km);
ρ_{c2},	second critical density (veh/km);
ρ_0,	initial density on the ring road (veh/km);
ω,	$= \Delta t/\Delta x$, ratio of time step to spatial mesh length;
ν,	fluid kinematic viscosity (m^2/s);
τ,	relaxation time (s);
τ_0,	relaxation time relevant to speed c_0 (m^2/s).

1 Introduction

Traffic flows have been widely studied due to the significant impacts on travel time and economic activities. Therefore, to ascertain characteristics and properties of traffic flows, many macroscopic traffic models have been developed, for instance, the Lighthill-Whitham-Richards model[1–2], the Euler model[3], the gas-kinetic-based model[4–5], the Navier-Stokes like model[6], the class of second-order models[7–8], and the generic model[9–10].

Greenberg[7] analyzed a class of second-order traffic models and showed that these models support stable oscillatory traveling waves typical of the waves observed on a congested roadway. The stable traveling waves arise as there is an interval of car spacing for which the constant solutions are unstable. These waves consist of a smooth part where both the velocity and spacing between successive cars are increasing functions of a Lagrange mass index.

To develop the conserved higher-order anisotropic traffic flow model[11], the approach to assign pseudo-density was proposed and applied. To show the properties of nonlinear traveling waves, the hyperbolic inviscid continuum traffic model was employed[12].

Borsche et al.[8] reviewed and numerically compared a special class of multi-phase traffic theories based on microscopic, kinetic, and macroscopic traffic models, and found that for all models but one, phase transitions can appear near bottlenecks depending on the local density and velocity of the flow.

By applying and extending methods from statistical physics and nonlinear dynamics to self-driven many-particle systems, Helbing[13] answered some questions about traffic flows, such as why are vehicles sometimes stopped by "phantom traffic jams" even though drivers all like to drive fast? What are the mechanisms behind stop-and-go traffic? Why are there several different kinds of congestion, and how are they related? Nagatani[14] reported that traffic systems display a surprisingly rich spectrum of spatial-temporal pattern formation phenomena. These phenomena can be explored by using the car-following models[15], the cellular automaton models[16–18], the gas-kinetic models, or the fluid-dynamical models[4–6].

Some notable studies about macroscopic traffic models can be found in Refs. [19]–[25], with the sensitivity of traffic flow to viscoelasticity reported recently by Smirnova et al.[26–27]. Time prediction, a relatively detail background has been given in Ref. [28]. Here to present a background briefly, two heuristic rules were examined by Chang and Mahmassani[29]. The rules were proposed for describing urban commuters' predictions of travel time as well as the adjustments of departure time in response to unacceptable arrivals in their daily commute under limited information. Some details for travel prediction can be found in Refs. [30]–[39], with some more recent work reported in Refs. [40]–[43].

In this paper, travel time through a ring road with a total length of 80 km is predicted numerically by a viscoelastic traffic model (VEM), in which the traffic pressure for the unfree flow case has a form similar to that reported in Ref. [28], but the pressure for the free flow is derived by assuming that the sound speed for the free flow case depends on the traffic density in some specific aspects, which ensures that the sound speed is exactly identical to the free flow speed on an empty road. The VEM uses the second critical density and speed to describe the fundamental diagram given by Fig. 1, in addition to the uses of the free flow speed, the braking distance in the unit of average vehicular length, the first critical density, and the jam density.

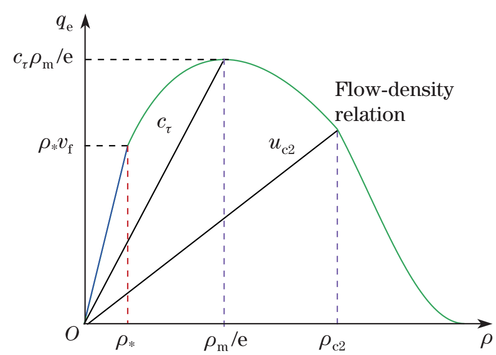

Fig. 1 Fundamental diagram

To make a comparison of the VEM, using the same forms of traffic pressure and traffic sound speed in the VEM, the open Navier-Stokes type model developed by Zhang[44] is employed to predict the travel time for providing the counterpart results. To calculate the local average speed for expressing the travel time and its root mean square (rms) value, a distinguishing time period named Δ_0 is preassigned.

The VEM and the numerical method are introduced before the section of model for comparison, after which is the section of results and discussion, with the conclusions summarized finally. The aim of the present paper is to develop the VEM to predict the travel time, and to investigate the drop of traffic flow rate, hysteresis phenomena, and distinguish strategies for travel time minimization.

2 Viscoelastic model

As the instantaneous traffic rate q is unequal to the equilibrium q_e, car drivers tend to adjust the moving speed so that the time headway can approach $1/q_e$ (see Ref. [45]). Such traffic selfadjusting behaviors have been studied by introducing the traffic viscosity and pressure in some high-order models[6,44,46].

Instantaneous variation of traffic rate is common in congested traffic flows, where the density is larger than the saturation one ρ_{s} ($= \rho_{\mathrm{m}}/\mathrm{e}$), as shown in Fig. 1. The interaction of vehicles in congested traffic is more intensive, leading to the occurrence of synchronized flow regime in which characterized by stop-and-go phenomena[47]. However, the flow returns to be homogeneous and stable for the denser case where the traffic speed is lower than the second critical speed corresponding to ρ_{c2}[48]. As time delay has been used to denote the external force of traffic flows, while relaxation and elastic processes are inherently related from points of view in fluid mechanics, it should be more reasonable to further include the elastic effect in traffic flow modeling. If only interaction of vicinity vehicles is considered, when interaction of vehicles between different lanes is neglected, the traffic flow rate and the density can be considered as one-dimensional variables.

For simplicity, we assume that (i) the ramp flow effect can be neglected; (ii) the road capacity is insensitive to vehicular drivers; (iii) the traffic flow satisfies a linear viscoelastic constitutive relation. The main reason supporting the third assumption is that in many high-order models, relaxation time which usually relates the elasticity and viscosity of fluids[49] has been used to define the driven force of vehicles, while for driver safety concern, vehicle motion may have a memory behavior.

In the viscoelastic modeling of traffic flows, the traffic pressure is employed. As reported by Flynn et al.[12], the pressure incorporates the effects of kinematic dispersion and the preventive driving needed to compensate for the relaxation time τ.

As reminded[25,50], there is no actual inter vehicular pressure or momentum flux. The pressure occurs in crush tests, or when vehicles are colliding. In traffic flows, there are some conduct rules that regulate vehicle acceleration/deceleration via drivers' reaction to road conditions. Those conduct rules could be determined in different ways, but usually they are incorporated into the equations in terms of local flow acceleration depending on flow conditions[51–52]. Being multiplied by the traffic density, the equations formally look like momentum transfer equations. Thus, virtual attraction or repulsion forces are introduced, which could be represented as a derivative of some function for one-dimensional flows. That function following the fluid flow analogy is named the traffic pressure. This point of view has been appropriately used in recent mathematical modeling[53].

In analogy to unsteady traffic flows, using the first-order approximation in the case of $N = 1$ rather than $N = 2$ as reported[22], the traffic flow stress can be expressed as

$$T = -p + G\tau B_1, \tag{1}$$

where G is the modulus of fluid elasticity. If the traffic speed is denoted by u, according to the work of Bogdanova et al.[25], $B_1 = 2u_x$, we have $\rho\nu = 2G\tau$, $\sigma = \nu\tau$, and $T = -p + \rho\nu u_x$.

In accordance to the existing high-order models[3–6,22,44,54–55], the forces acting on vehicular clusters have a general form of

$$F = (q_{\mathrm{e}} - q)/\tau + T_x,$$

where the subscribe e represents the relevant variables under the equilibrium traffic state, q_{e} is the traffic flow rate under the equilibrium traffic state, which can be seen as a function of traffic density, with the form being related to the free flow speed v_{f}, the first critical density ρ_*, the second critical density ρ_{c2}, the speed u_{c2}, the vehicular jam density ρ_{m}, and the vehicular moving speed parameter c_τ as reported (see Kiselev et al.[56]). T_x is the relevant surface force related to the traffic stress. For $N = 1$, we have

$$F = (q_{\mathrm{e}} - q)/\tau - p_x + ((2G\tau)u_x)_x. \tag{2}$$

At the second critical density $\rho_{\rm c2}$, the traffic flow has a speed $u_{\rm c2}$. When the second critical speed is used to define a ratio $\Lambda = c_\tau/u_{\rm c2}$, the traffic fundamental diagram shown in Fig. 1 can be written as

$$q_{\rm e} = \begin{cases} v_{\rm f}\rho, \quad \rho \leqslant \rho_*, \\ -c_\tau \rho \ln(\rho/\rho_{\rm m}), \quad \rho_* < \rho \leqslant \rho_{\rm c2}, \\ B\rho(1 - {\rm sech}(\Lambda \ln(\rho/\rho_{\rm m}))), \quad \rho_{\rm c2} < \rho \leqslant \rho_{\rm m}, \end{cases} \tag{3}$$

where

$$\rho_* = \rho_{\rm m}(1 + X_{\rm br}/l)^{-1}, \quad \rho_{\rm c2}/\rho_{\rm m} = \exp(-1/\Lambda), \quad c_\tau = v_{\rm f}/\ln(1 + X_{\rm br}/l),$$
$$B = u_{\rm c2}/(1 - {\rm sech}(\Lambda \ln(\rho_{\rm c2}/\rho_{\rm m}))), \quad {\rm sech}(\Lambda) \equiv 1/\cosh(\Lambda),$$

l denotes the average length of vehicles, and $X_{\rm br}$ represents the braking distance depending on the free-flow speed $v_{\rm f}$. Relevant to $\frac{\partial q_{\rm e}}{\partial \rho} = 0$, the saturation density $\rho_{\rm s}$ located in the density range $\rho \in (\rho_{\rm s}, \rho_{\rm c2})$ is exactly equal to $\rho_{\rm m}/{\rm e}$, where ${\rm e} = 2.718\,28$ is the natural number. As previously reported[22], the second critical speed is about 15 m/s. Corresponding to this speed value, the value of the second critical density can be made sure. Since $1/{\rm e}$ is certainly in the range from $1/3$ to 0.618, it implies that the fundamental curve described by Eq. (3) fits with the analytical result in Ref. [57], which is to some extent feasible and applicable. The $X_{\rm br}$ dependent fundamental diagram plays a crucial role in traffic flow modeling and numerical simulation[58].

As reported[25], the traffic pressure p is proportional to the reciprocal of spatial headway $1/\rho - l$. With the jam density denoted by $\rho_{\rm m}$, it can be written as

$$p = K(\rho/(1 - \alpha(\rho/\rho_{\rm m}))), \tag{4}$$

where K is a model parameter, and $\alpha = l\rho_{\rm m}$ with l representing the average length of vehicles. To a certain extent, the definition of traffic pressure is reasonable[28]. Using the definition of sound speed in classical mechanics, the traffic sound speed is

$$c = \sqrt{\frac{\partial p}{\partial \rho}} = K^{1/2}/(1 - \alpha\rho/\rho_{\rm m}). \tag{5}$$

If the traffic sound speed at the second critical density is just equal to c_τ as reported[59], an explicit expression for K is

$$K = c_\tau^2(1 - \alpha\rho_{\rm c2}/\rho_{\rm m})^2.$$

However, remembering the unfavourable comment of Daganzo[60], the specific traffic stoppage problem must be carefully faced. Apart from using the geometric average at the particular point at which the traffic density has an abrupt jump from the upstream zero to the downstream completely jammed value $\rho_{\rm m}$, here we suggest to use a definite sound speed exactly being equal to the free flow speed on the empty road. This implies that the traffic pressure described above needs to be improved. Hence, we assume that the traffic pressure on the empty road is zero, and the sound speed under free flow conditions satisfies some specific forms,

$$c^2 = c_*^2 + B_*(\rho - \rho_*)^4, \quad \rho \leqslant \rho_*, \tag{6}$$

where

$$c_*^2 = K/(1 - \alpha\rho_*/\rho_{\rm m})^2, \quad B_* = (v_{\rm f}^2 - c_*^2)/\rho_*^4. \tag{7}$$

Therefore, by integrating the square of sound speed ($p = \int_0^\rho c^2 {\rm d}\rho$), the traffic pressure can be rewritten as

$$p = \begin{cases} c_*^2\rho + \dfrac{1}{5}B_*(\rho_*^5 + (\rho - \rho_*)^5), \quad \rho \leqslant \rho_*, \\ K(\rho/(1 - \alpha(\rho/\rho_{\rm m}))) + B_0, \quad \text{otherwise} \end{cases} \tag{8}$$

with the constant

$$B_0 = c_*^2\rho_* + B_*\rho_*^5/5 - K(\rho_*/(1-\alpha(\rho_*/\rho_{\mathrm{m}}))) \tag{9}$$

used just for the pressure continuity at the density ρ_*. The corresponding sound speed can be rewritten as

$$c = \begin{cases} \sqrt{c_*^2 + B_*(\rho-\rho_*)^4}, & \rho \leqslant \rho_*, \\ K^{1/2}/(1-\alpha(\rho/\rho_{\mathrm{m}})), & \text{otherwise}. \end{cases} \tag{10}$$

The traffic pressure given by Eq. (8) comes from the careful consideration of the specific traffic stoppage problem[60], and it is different from the form in Ref. [12],

$$p \equiv -\beta_0(\rho + \ln(\rho_{\mathrm{m}} - \rho)),$$

where β_0 is a positive parameter with the unit of $\mathrm{m}^2/\mathrm{s}^2$.

To express τ explicitly, supposing $c\tau = $ const., and denoting the relaxation time at $\rho_{\mathrm{c}2}$ by $\tau_0 = l_0/c_\tau$ with the traffic length scale l_0, we have[25]

$$\tau = \begin{cases} \tau_0 c_\tau/c, & \rho \leqslant \rho^*, \\ \tau_0(1-\alpha\rho/\rho_{\mathrm{m}})/(1-\alpha\rho_{\mathrm{c}2}/\rho_{\mathrm{m}}), & \text{otherwise}. \end{cases} \tag{11}$$

Obviously, the relaxation time τ decreases linearly with the traffic density.

Therefore, using the expressions (2), (3), and (4), according to the mass and momentum conservations of vehicular movement, using the right-subscript of a variable to denote its partial derivative, we obtain the present viscoelastic traffic model in the following form:

$$\begin{cases} \rho_t + q_x = 0, \\ \rho(u_t + uu_x) = R \end{cases} \tag{12}$$

with R satisfying

$$R = (q_{\mathrm{e}} - q)/\tau - c^2\rho_x + ((2G\tau)u_x)_x, \tag{13}$$

where $c^2 = \frac{\partial p}{\partial \rho}$.

Note that the model has used the pressure gradient p_x/ρ to describe the traffic acceleration R/ρ. This means that negative speeds in the solutions can possibly occur[54], causing the development of anisotropic higher-order traffic flow models[61–62].

In the present VEM, in addition to the note[28] that the term $(q_{\mathrm{e}} - q)/\tau$ can lower the probability of negative speed occurrences, it is necessary to remind that the assumption of the sound speed at zero density ($c = v_{\mathrm{f}}$ at $\rho = 0$) is certainly helpful to present a favourable approach for modeling the specific traffic stoppage problem particularly discussed by Daganzo[60], as it makes all the elements in the first column of Jacobian matrix as seen in Eq. (15) become zero. As a result, the traffic flow rate is totally not sensitive to density heterogeneity.

3 Numerical method

Using $R_1 = R + c^2\rho_x$ instead of R, the governing equations (12) and (13) become

$$\frac{\partial \boldsymbol{U}}{\partial t} + \frac{\partial \boldsymbol{F}(U)}{x} = \boldsymbol{S}, \tag{14}$$

where

$$\boldsymbol{U} \equiv (U_1, U_2)^{\mathrm{T}} = (\rho, q)^{\mathrm{T}}, \quad \boldsymbol{F}(\boldsymbol{U}) \equiv (F_1, F_2)^{\mathrm{T}} = (q, q^2/\rho + p)^{\mathrm{T}},$$
$$\boldsymbol{S} \equiv (S_1, S_2)^{\mathrm{T}} = (0, R_1)^{\mathrm{T}}$$

with the superscript T representing the vector transpose.

The eigenvalues of Eq. (14) λ_k $(k=1,2)$ are $\lambda_1 = u - c$ and $\lambda_2 = u + c$, where the Jacobian matrix is

$$\boldsymbol{A} = \begin{pmatrix} \dfrac{\partial F_1}{\partial U_1} & \dfrac{\partial F_1}{\partial U_2} \\ \dfrac{\partial F_2}{\partial U_1} & \dfrac{\partial F_2}{\partial U_2} \end{pmatrix} = \begin{pmatrix} 0 & 1 \\ -u^2 + c^2 & 2u \end{pmatrix}. \tag{15}$$

While some believe that the eigenvalue should not exceed the traffic speed, the present viscoelastic model uses non-Newtonian fluid flow analogy, such that the traffic speed involves vehicular cluster rather than a single car. The eigenvalue limit is irrelevant. In fact, an eigenvalue represents a propagation speed of traffic wave (shock or rarefaction wave) and it is not necessary to set a limit for the propagation speed with respect to the speed of Brownian motion of fluid molecular particles.

The total variation diminishing (TVD) scheme developed by Ref. [63] is adopted to solve the governing equation (14). Using the right-superscript 'n' to denote the variables at the time level n, the source term S_2 at the time level $n+1/2$ can be expressed by a linear expansion,

$$S_2^{n+1/2} = S_2^n + \frac{1}{2}\Big(\frac{\partial S_2}{\partial \rho}\Big)^n \delta\rho^n + \frac{1}{2}\Big(\frac{\partial S_2}{\partial q}\Big)^n \delta q^n, \tag{16}$$

where

$$\delta\rho^n = \rho^{n+1} - \rho^n, \quad \delta q^n = q^{n+1} - q^n.$$

Represent the speed and length scales respectively by v_0 and Δx $(= l_0)$ so that the time scale is $t_0 = l_0/v_0$. For simplicity, use the scaled variables as the same as unscaled so that the form of dimensionless expression

$$S_2 = R_1 = R + c^2\rho_x + \sigma_1 q u = (q_{\mathrm{e}} - q)/\tau + ((2G\tau)u_x)_x + \sigma_1 q u$$

keeps the same. By simply neglecting the roles of viscous term $((2G\tau)u_x)_x$ in the linear expansion, we have

$$\frac{\partial S_2}{\partial \rho} = \tau^{-1}\Big(\frac{\partial q_{\mathrm{e}}}{\partial \rho}\Big), \quad \frac{\partial S_2}{\partial q} = -\tau^{-1}. \tag{17}$$

The linearization of S_2 is useful to the accuracy of temporal discretization and the numerical stability of the TVD scheme, which has the form of

$$\delta \boldsymbol{U}_i^n = -\omega(\widehat{\boldsymbol{F}}_{i+1/2} - \widehat{\boldsymbol{F}}_{i-1/2}) + (\Delta t)\boldsymbol{S}_i^n + \frac{\Delta t}{2}\Big(\frac{\partial \boldsymbol{S}}{\partial \boldsymbol{U}}\Big)_i^n \delta \boldsymbol{U}_i^n, \tag{18}$$

where $\delta \boldsymbol{U}_i^n = \boldsymbol{U}_i^{n+1} - \boldsymbol{U}_i^n$, $\Delta t = t^{n+1} - t^n$, and $\omega = \Delta t/\Delta x$ is the ratio of time step to mesh size, defined by

$$\omega = C_{\mathrm{FL}}/\max|\lambda_{k,i+1/2}|, \quad k = 1,2, \quad i = 0,1,2,\cdots,I_{\max}-1, \tag{19}$$

where $\lambda_{k,i+1/2}$ is the kth eigenvalue for $\boldsymbol{A}$ at $x_{i+1/2}$, $I_{\max}$ is the maximum mesh number, and the Courant number C_{FL} is taken as 0.4 in the numerical tests[64]. The numerical flux $\widehat{\boldsymbol{F}}_{i+1/2}$ can be calculated using the eigen vectors of Jacobian matrix $\boldsymbol{A}$. The calculation of $\widehat{\boldsymbol{F}}_{i+1/2}$ involves evaluating the coefficients of viscous term $Q_k(z)$ with an artificial parameter ϵ_k, as reported previously[65–66].

4 Model for comparison

To make a comparison, the traffic model developed by Zhang[44] is adopted. Assume $\tau_0/\tau = c/c_0$ and $l_0 = c_0\tau_0$ similar to the work[27]. The model of Zhang[44] can be written as

$$\begin{cases} \rho_t + q_x = 0, \\ q_t + (q^2/\rho + p + ((2\beta c_0)(c/c_0))(q/\rho))_x = R_2, \\ R_2 = \Big(\dfrac{q_\mathrm{e} - q}{\tau_0}\Big)(c/c_0) + ((2\beta c_0)(c/c_0)\rho)(q/\rho)_{xx} + (q/\rho)((2\beta c_0)(c/c_0)\rho)_x, \end{cases} \tag{20}$$

where the equilibrium flow rate q_e satisfies Eq. (3), and the traffic pressure is expressed by Eq. (4), with the sound speed ratio c/c_0 described by Eq. (5). The parameter β is defined by

$$\beta = \frac{\nu}{2\tau_0 c_0^2}. \tag{21}$$

Defining

$$E_2 = (2\beta c_0)(c/c_0)(q/\rho) \tag{22}$$

and using the form of Eq. (14), now for the model of Zhang[44], we have

$$F_2 = q^2/\rho + p + E_2, \tag{23}$$

which indicates that the Jacobian matrix should contain the influence of E_2. When the sound speed ratio c/c_0 is density dependent, we have

$$\begin{cases} \dfrac{\partial E_2}{\partial \rho} = (2\beta c_0)\Big(\dfrac{\partial (c/c_0)}{\partial \rho}\Big(\dfrac{q}{\rho}\Big) + (c/c_0)\Big(-\dfrac{q}{\rho^2}\Big)\Big), \\ \dfrac{\partial E_2}{\partial q} = (2\beta c_0)(c/c_0)\Big(\dfrac{1}{\rho}\Big). \end{cases} \tag{24}$$

For the source term $S_2 = R_2$, the discretization of $((2\beta c_0)(c/c_0)\rho)_x$ is done by a second-order upwind scheme[67]. The solution method for Eq. (20) is also TVD[63] as described in Section 3.

5 Results and discussion

5.1 Simulation parameters

To predict traffic density dependence of the travel time T_t and its rms value T_t', by using the traffic fundamental diagram in Fig. 1, the traffic pressure and traffic sound speed ratio in Fig. 2, and the traffic flow parameters in Table 1 for traffic flows on the ring road given by Fig. 3, numerical tests based on the model of Zhang[44] and the present VEM are conducted.

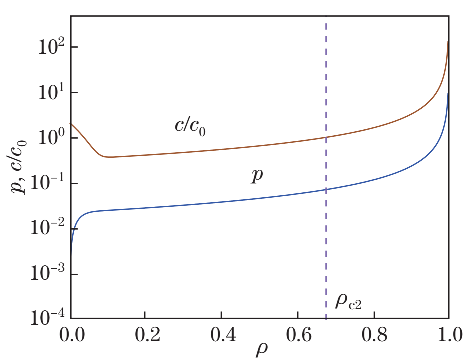

Fig. 2 Traffic pressure p and traffic sound speed ratio c/c_0 versus density ρ, where ρ is measured by jam density ρ_m, and p has unit of $\rho_\mathrm{m} v_\mathrm{f}^2$

Table 1 Parameters of traffic flow on ring road

$v_{\mathrm{f}}/(\mathrm{km}\cdot\mathrm{h}^{-1})$	$\rho_{\mathrm{m}}/(\mathrm{veh}\cdot\ \mathrm{km}^{-1})$	$X_{\mathrm{br}}/\mathrm{m}$	l/m	L/km	l_0/m
80	172	45	5.8	80	100
ρ_*	ρ_{s}	ρ_{c2}[1]	$v_0/(\mathrm{m}\cdot\mathrm{s}^{-1})$	$c_0/(\mathrm{m}\cdot\mathrm{s}^{-1})$	τ_0/s
0.114	0.368	0.666	2.537	10.24	9.765
γ	Λ	X_A/km	X_B/km	X_C/km	X_D/km
0.031 25	2.458	10	30	50	70

[1] ρ_*, ρ_{s}, and ρ_{c2} are measured by jam density ρ_{m}.

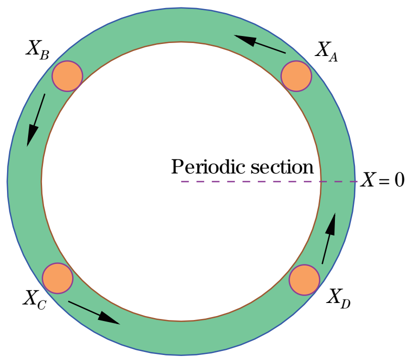

Fig. 3 Schematic diagram of ring traffic flow with four initial jams located at X_J $(J = A, B, C, D)$

The initial density on the ring road is

$$\rho(0,x) = \begin{cases} 1.0, & x \in [X_J - 1/2, X_J + 1/2], \\ \rho_0, & \text{otherwise}, \end{cases} \tag{25}$$

where $q(0,x) = q_{\mathrm{e}}(\rho(0,x))$, and the values of X_J $(J = A,\ B,\ C,\ D)$ are given in the bottom line of Table 1. In the second column of Table 1, it is seen that $\Lambda = 2.458$, a value relevant to the second critical speed $u_{\mathrm{c2}} = 15\,\mathrm{km/h}$[22]. The viscoelasticity $\gamma = \frac{2G(\tau_0 v_0)}{l_0^2}\frac{t_0}{q_0}$ in the first column of Table 1 is assumed to be 0.031 25, a value corresponding to $\beta = 3.871 \times 10^{-3}$ in the model of Zhang[44].

The initial jams are strictly assumed to be positioned at four grid points X_J $(J = A, B, C, D)$ (see Fig. 3). The behavior of these jams' propagation is extremely dependent on the value of ρ_0, in addition to the sensitive influence from the viscoelasticity γ as reported[27].

The travel time T_{t} on the ring road is calculated with the traffic flow speed u and the road length L, when the total space grid number is $N = 801$. According to $L = (N-1)l_0$, the road length equals 80 km exactly. As reported[28], if the instantaneous travel time is

$$T_{\mathrm{t}}(t) = \sum_{k=1}^{N-1} l_0/\overline{u}_k(t), \tag{26}$$

where

$$\overline{u}_k(t) = \frac{1}{\Delta_0}\int_{t-\Delta_0}^{t} u_k(\xi)\mathrm{d}\xi,$$

in which $\Delta_0 = 7.5$ min, it is a pre-assigned distinguishing period for time average.

As traffic jam propagations can result in the variations of traffic speed and density, we have to predict the mean travel time T_{tav} by averaging $T_{\mathrm{t}}(t)$ in the period $t \in (t_0, t_{\mathrm{end}})$, and calculate the relevant rms T_{t}'. Hence, we have

$$T_{\mathrm{tav}} = \frac{1}{t_{\mathrm{end}} - t_0} \int_{t_0}^{t_{\mathrm{end}}} T_{\mathrm{t}}(\xi) \mathrm{d}\xi, \tag{27}$$

$$[T_{\mathrm{t}}']^2 = \frac{1}{t_{\mathrm{end}} - t_0} \int_{t_0}^{t_{\mathrm{end}}} (T_{\mathrm{t}}(\xi) - T_{\mathrm{tav}})^2 \mathrm{d}\xi. \tag{28}$$

In the numerical tests, it is also assumed the product $c\tau$ is a constant. Figure 2 shows the traffic pressure and traffic sound speed ratio c/c_0, where c_0 is the traffic sound speed at the second critical density ρ_{c2}. The blue-colored curve indicates that the traffic pressure increases with the density monotonically. It is zero for the specially empty case with no vehicles on the road, i.e., $\rho = 0$. It is $p_{\mathrm{m}} = 10.004$ for the case $\rho = 1$. For all free flow states $\rho \leqslant \rho_*$ with $\rho_* = 0.114$, the traffic pressure p holds a value less than 2.557%. For under-saturated traffic flows $\rho \in (\rho_*, \rho_{\mathrm{s}})$, with the saturation point $\rho_{\mathrm{s}} = 1/\mathrm{e} \approx 0.368$ where $\mathrm{e} = 2.718\,28$, p holds a value in the range $(2.557\%, 3.643\%)$. For over-saturated traffic flows having a density less than the second critical density $\rho_{\mathrm{c2}} = 0.666$, that is, $\rho \in [\rho_{\mathrm{s}}, \rho_{\mathrm{c2}})$, p has a value located in the range $[3.643\%, 6.986\%)$. It is seen that the second critical pressure $p_{\mathrm{c2}} = 6.986\%$, beyond which the pressure increases rapidly with the traffic density. The pressure reaches a value of about 1.073 for $\rho = 0.98$, and about 10 for the completely jammed case $\rho = 1$.

The brown-colored curve in Fig. 2 denotes the variation of traffic sound speed c/c_0 with the density. It is seen that for $\rho = \rho_{\mathrm{s}}$, $c/c_0 = 0.531$.

5.2 Traffic flow patterns

Traffic flow patterns are given by density spatial-temporal evolutions for $\rho_0 = 0.1, \rho_{\mathrm{s}}$, and ρ_{c2}, as shown in Figs. 4(a)–4(c), where the patterns obtained by using the model of Zhang[44] are located on the left, with that based on the present VEM on the right. In Fig. 4(a), it is seen that both models have predicted that the four initial traffic jams become forward moving bottlenecks, and the trajectories of these bottlenecks are straight lines, with the line-slope representing the moving speed, apparently dependent on the traffic model employed. Using the VEM model, the slope corresponds to a bottleneck moving speed of about 30.4 km/h. With the model of Zhang[44], the bottleneck moving speed is about 30.2 km/h, indicating that both are almost identical. The traffic patterns given by Fig. 4(a) are the solutions to the initial value problem well-posed, as discussed by Daganzo[68].

Figure 4(b) shows the traffic flow patterns for $\rho_0 = \rho_{\mathrm{s}}$. The spatial-temporal evolutions of initial jams spread backward at a speed of about –9.6 km/h, which is rather close to the jam propagation speed –11 km/h as predicted by the gas-kinetic traffic model[4]. Between the initial jams, spontaneously generated jams can be observed, which are similar to those narrow jams found in the data measured on German highways[47]. They start to move forward, but with the increase in the jam intensity due to vehicle aggregation, the propagation direction gradually changes to the backward. At the time of about $t = 0.66$ h, the spontaneous jams nearest to the backward spreading initial jam, catch up and merge with it, causing the propagating direction of merged jams' changed. Because of the interaction of traffic waves, commonly named traffic shocks and rarefaction waves, the ring traffic flow for $\rho_0 = \rho_{\mathrm{s}}$ gradually develops to the stop-and-go mode. Even though we use the same pressure and sound speed curves as seen in Fig. 2 in numerical tests, the traffic flow patterns based on the two traffic models have some differences certainly, but not large.

Moreover, for the ring traffic flow at the second critical point, the spacio-temporal evolutions obtained from both traffic models are exteriorly the same, as shown in Figs. 4(e) and 4(f). The initial jams propagate backward at a speed of 28.2 km/h, relevant to the model of Zhang[44] and the present model. The predicted propagation speed of jams is approximately $2u_{\mathrm{c2}}$. Most vehicles run on the ring road at u_{c2} =15 km/h, with those in the jams moving at a slower speed.

The traffic flow patterns shown in Figs. 4(e) and 4(f) belong to a special type of stop-and-go mode, corresponding to congested scenarios in real traffic, as occurred in some road segment of urban region occurred in the time to work around 7:00 a.m. or in the time to get off work around 6:00 p.m.

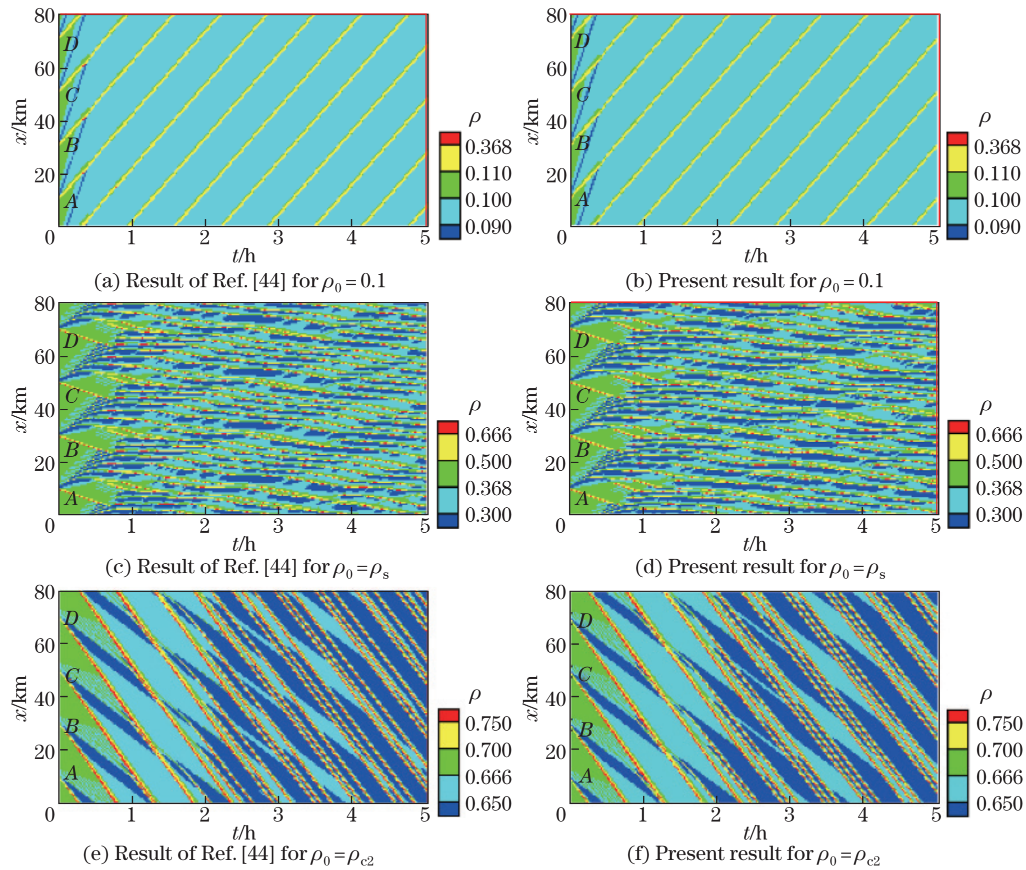

Fig. 4 Spatial-temporal evolutions of traffic density in ring road (color online)

It is seen that the patterns on the ring road are obviously dependent on the initial density ρ_0. The propagation speeds of jams depend on the wave interaction and the fundamental diagram used in the numerical test, as reported in Ref. [68] and in the recent studies[9–11,27]. The specific property of the fundamental diagram given by Eq. (3) is that it has a clear use of second critical density and speed. In the numerical tests, the second critical speed is fixed at $u_{c2} = 15\,\mathrm{km/h}$.

5.3 Distributions of density and speed

The consistent properties of flow pattern illustrated by comparing the left and right parts of Fig. 4 have validated the reliability and applicability of the present model to some extent, as the model of Zhang[44] by using the car-following rule is a open Navier-Stokes type. To show the differences in numerical solutions related to the two traffic models in more details, distributions of traffic density and speed at the position $x = 40\,\mathrm{km}$ are shown in Figs. 5(a) and 5(b), Figs. 6(a) and 6(b), and Figs. 7(a) and 7(b) for $\rho_0 = 0.1$, ρ_s, and ρ_{c2}, respectively.

In Figs. 5(a) and 5(b), the solid curves denote the density and speed distributions at $t = 0.5\,\mathrm{h}$ based on the present VEM, with the dash-dotted curves representing the relevant density and speed distributions based on the model of Zhang[44]. The symbols A and D are just used to indicate the peaks of density and negative pulses of speed, corresponding to the initial jams located at X_A or X_D. The distributions of the traffic density either dash-doted or solid are exactly consistent with the traffic pattern given by Fig. 4(a). In the third line of Table 1, we find $X_A = 10\,\mathrm{km}$ and $X_D = 70\,\mathrm{km}$. By seeking the space positions of the peaks shown by solid curve, remembering that the time period length is 0.5 h, it can be predicted that the speed of forward moving bottlenecks is about 30.4 km/h. Similarly, the relevant speed of the moving bottlenecks predicted by the model of Zhang[44] is 30.2 km/h, as mentioned in the foregoing subsection 5.2.

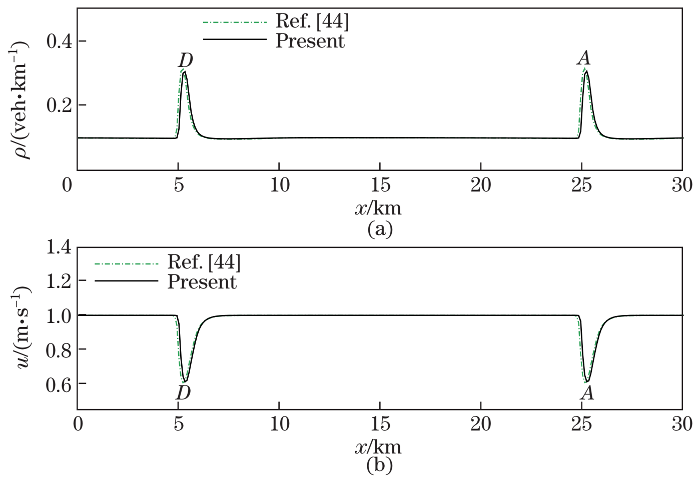

Fig. 5 Comparison of (a) density and (b) speed distributions at $t = 0.5\,\mathrm{h}$ and $x \in (10, 30)$ in the case of $\rho_0 = 0.1$. Note that ρ and u have units of ρ_m and v_f, respectively

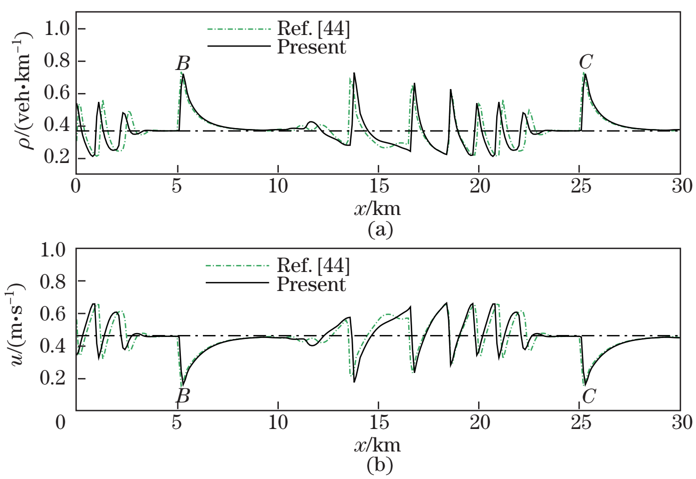

Fig. 6 Comparison of (a) density and (b) speed distributions at $t = 0.5\,\mathrm{h}$ and $x \in (0, 30)$ in the case of $\rho_0 = \rho_\mathrm{s}$

However, in Figs. 6(a) and 6(b), the distributions of density and speed for $\rho_0 = \rho_\mathrm{s}$ at time $t = 0.5\,\mathrm{h}$ are labeled by symbols B and C to show initial positions of the initial jams located at X_B and X_C, respectively. The density distribution given by solid curve has provided accurate evidence for determining the backward propagating speed of initial jams, which is about −9.6 km/h. The distributions of density and speed show that there exist six spontaneously generated traffic jams between the initial jams located at B and C. This spontaneous generation of traffic jams was found by Kerner[47] in data measured in German highways. The spontaneous phenomenon proved by numerical tests suggests that the curves of traffic pressure and sound speed given by Fig. 2 have potential application.

As shown in Figs. 7(a) and 7(b), the exterior overlapping of distribution curves of density and speed for $\rho_0 = \rho_{c2}$ is a reflection of consistency in the traffic patterns given by the left and right parts of Fig. 4(c). Relatively accurate calculation reveals that the backward propagating speed of the initial jams based on the present model (~ 28.2 km/h) is the same as the propagation speed value predicted by the model of Zhang[44].

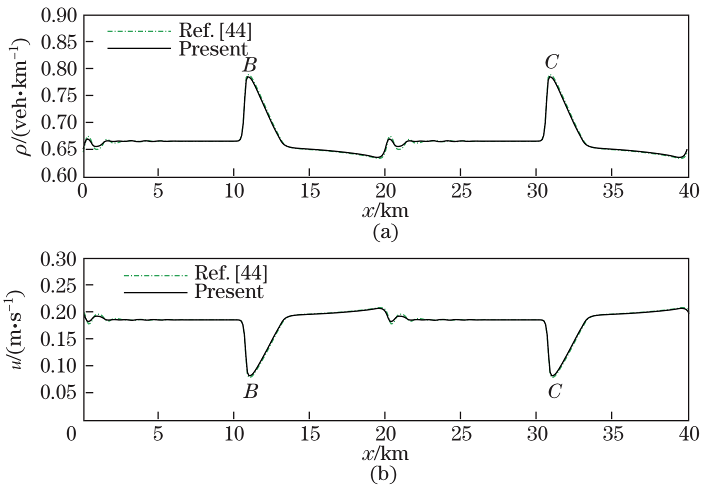

Fig. 7 Comparison of (a) density and (b) speed distributions at $t = 0.5$ h and $x \in (0, 40)$ in the case of $\rho_0 = \rho_{c2}$

Impacted by the spatial-temporal evolutions of traffic waves, for the ring traffic flow in the case of $\rho_0 = \rho_s$, the density and speed distributions on the ring road at $t = 0.25$ h and 0.5 h have different properties, as shown in Figs. 8(a) and 8(b). For $t = 0.25$ h, the distributions of density and speed are shown by green-dashed curves. In comparison with the black-solid curves for $t = 0.5$ h, the total number of density peaks increases, and the number of spontaneously generated jams and their heights increase with the flow time.

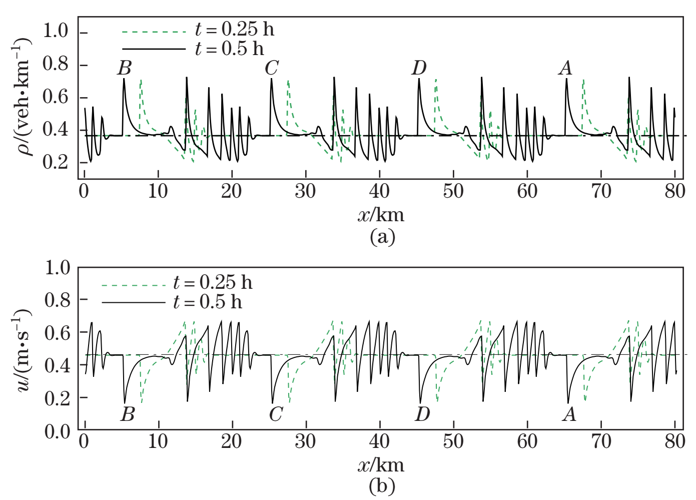

Fig. 8 Distributions of (a) density and (b) speed on ring road at $t = 0.25$ h, 0.5 h in the case of $\rho_0 = \rho_s$

5.4 Evolutions of density and speed

For three values of ρ_0, the temporal evolutions of the traffic flow speed and density at $x = 40$ km can be seen in Figs. 9(a)–9(c). When ρ_0 is slightly less than ρ_*, Fig. 9(a) indicates that the common traffic mode on the ring road is free flow state, vehicles moving at the speed v_{f}, excluding those vehicles in moving bottlenecks whose moving speed can be calculated by simply predicting the ring road travel time for an initial jam. For instance, the time of the first occurrence of the bottleneck labeled by B is about $t = 0.347\,4$ h, while the time of the second occurrence is about $t = 2.845$ h, hence for the bottleneck labeled by B, whose ring road travel time is 2.496 h, equivalently indicating that the forward propagation speed is about 32.03 km/h, a speed value being close to 30.4 km/h estimated using Fig. 4(a).

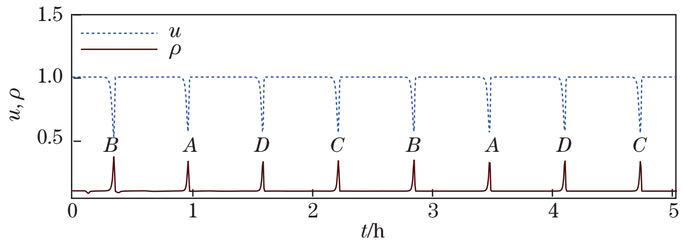

(a) $\rho_0 = 0.1$

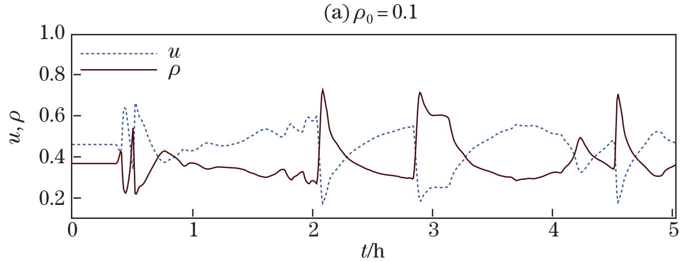

(b) $\rho_0 = 0.368$

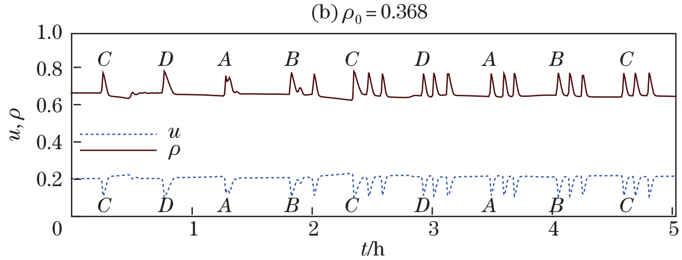

(c) $\rho_0 = 0.666$

Fig. 9 Temporal evolutions of traffic flow speed and density at $x = 40$ km for (a) $\rho_0 = 0.1$, (b) $\rho_0 = \rho_{\mathrm{s}}$, and (c) $\rho_0 = \rho_{\mathrm{c}2}$

Figure 9(b) shows that for $\rho_0 = \rho_{\mathrm{s}}$, there are oscillations accompanied by several peaks and negative pulses on the evolution curves of density and speed, causing by the propagation and interaction of traffic waves. As shown in Fig. 4(b), the merges of initial jams with spontaneously generated jams, and interaction between jams and rarefaction waves, have presented bridges of changing jams intensity and propagation direction. The speed oscillations at $x = 40$ km reflects the nonlinearity of governing equation for the traffic speed. It implies that the predicted travel time through the rind road on the basis of traffic models may have uncertainty to some extent.

Being consistent with the traffic pattern illustrated by Fig. 4(c), and labeling the density peaks and speed negative pulses by symbols according to their initial jams located at X_J ($J = A,\ B,\ C,\ D$), observing at the section $x = 40$ km, one can see the evolutional curves of density and speed for $\rho = \rho_{\mathrm{c}2}$ as shown in Fig. 9(c). For the congested traffic flow, usually moving at the second critical speed $u_{\mathrm{c}2} = 15$ km/h, the initial jams propagate backward at a speed of about 28.2 km/h. Furthermore, the second occurrence of any initial jams generally accompanied by a spontaneously generated jam, clearly suggests that traffic jams have a cleavage property, in addition to the mergence with a spontaneously jam nearest[47] due to colliding.

5.5 Comparison with measured data

The instantaneous traffic speed u at $x = 40\,\mathrm{km}$ is plotted as a function of traffic density in Figs. 10(a)–10(c), where the instantaneous equilibrium speed ($u_{\mathrm{e}} = q_{\mathrm{e}}/\rho$) at $x = 40\,\mathrm{km}$ is labeled by unfilled blue-triangles, and the measured data in Refs. [69] and [70] are labeled by unfilled black squares.

In Fig. 10(a), the instantaneous traffic speed for $\rho_0 = 0.2$ varies in the range of measured data. It can be seen that for the under-saturated ring traffic flow $\rho_0 < \rho_{\mathrm{s}}$, there are more unfilled green circles above the unfilled blue-triangles vehicles, indicating that for over-saturated scenarios ($\rho > \rho_{\mathrm{s}}$), vehicles usually have a larger instantaneous speed than the equilibrium value.

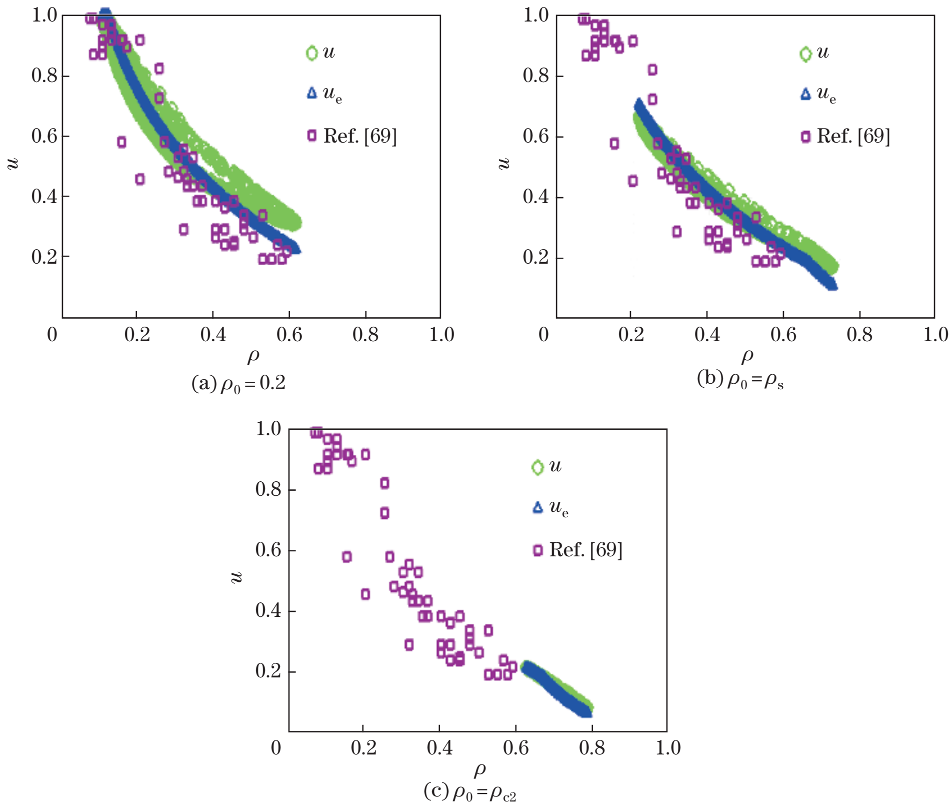

Fig. 10 Comparison of traffic speed with existing measured data at $x = 40\,\mathrm{km}$ for (a) $\rho_0 = 0.2$, (b) $\rho_0 = \rho_{\mathrm{s}}$, and (c) $\rho_0 = \rho_{\mathrm{c2}}$. The observation data are obtained from McShane et al.[69], and the jam density for normalisation is supposed to be 124 veh/km (color online)

Figure 10(b) shows the variations of instantaneous and equilibrium traffic speeds with density for the case of $\rho_0 = \rho_{\mathrm{s}}$ at $x = 40\,\mathrm{km}$.

The instantaneous speed varies in the density range $\rho \in [0.215\,0, 0.728\,0]$, and the speed is usually in good agreement with the measured data.

Figure 10(c) shows the variations of speeds with density for the case of $\rho_0 = \rho_{\mathrm{c2}}$ at $x = 40\,\mathrm{km}$. The rarefactive waves can lead to the traffic density in blue-colored regions downstream the jams as low as $0.625\,3$. Moreover, the vehicle aggregation can lead to the density in jams to keep a value as high as 0.788. As can be seen in Fig. 10(c), the dependency of instantaneous speed on density agrees with that of the equilibrium speed quite well, but the relevant measured data are less collected.

5.6 Travel time

The travel time T_{t} is calculated by introducing a time averaged speed $\overline{u}_k(t)$, when the time average is based on the period $\Delta_0 = 7.5$ min. The use of Δ_0 can avoid the occurrence of $\overline{u}_k(t) = 0$. Figure 11 shows the temporal evolution of T_{t} for the cases of $\rho_0 = 0.1$, ρ_{s}, and ρ_{c2}. These evolution curves of T_{t} are corresponding to the average value T_{tav} and its rms value T_{t}' shown by bold numbers in Table 2.

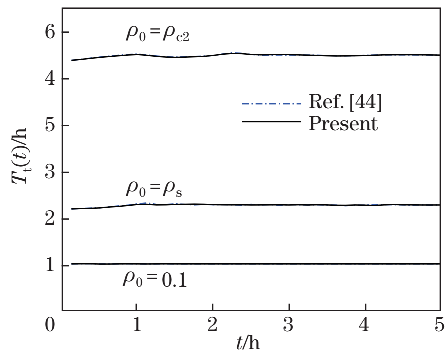

Fig. 11 Temporal evolution of travel time T_{t} through ring road at three values of ρ_0

Table 2 Traffic density dependence of travel time and its rms value

ρ_0	Present		Ref. [44]		ρ_0	Present		Ref. [44]	
	T_{tav}/h	a^*T_{t}'/h	T_{tav}/h	aT_{t}'/h		T_{tav}/h	aT_{t}'/h	T_{tav}/h	aT_{t}'/h
0.100	**1.017**	**0.070**	**1.027**	**0.087**	0.600	4.271	0.241	4.272	0.291
0.200	1.352	0.531	1.354	0.507	0.633	4.787	0.316	4.790	0.384
0.300	1.867	1.167	1.874	1.483	**0.666**	**5.488**	**3.054**	**5.491**	**2.984**
0.368	**2.276**	**2.509**	**2.279**	**2.596**	0.700	6.521	1.437	6.523	1.566
0.400	2.453	2.152	2.459	2.148	0.750	9.159	0.079	9.159	0.079
0.450	2.777	1.177	2.779	1.297	0.800	14.174	0.148	14.174	0.148
0.500	3.164	0.785	3.167	0.661	0.840	22.209	0.285	22.209	0.285
0.550	3.654	0.269	3.652	0.541	0.880	39.957	0.594	39.957	0.580

*Here, $a = 100$, used as a factor merely for the convenience of illustration

Being relevant to the values given by Table 2, the variations of mean travel time T_{tav} and its rms value T_{t}' with the ring road traffic density are shown in Figs. 12(a) and 12(b). For $\rho_0 = 0.1$, the mean travel time T_{tav} is about 1.02 h, with a negligible delay time 0.02 h. For $\rho_0 = \rho_{\mathrm{s}}$, $u_{\mathrm{e,s}} = 0.460\,9 v_{\mathrm{f}}$, on the basis of the VEM model and the model of Zhang[44], the travel time T_{tav} are, respectively, 2.276 h and 2.279 h, being relevant to $T_{\mathrm{t}}' = 2.509 \times 10^{-2}$ h, 2.596×10^{-2} h. The mean travel time is almost equal to $T_{\mathrm{tav,s}} = L/u_{\mathrm{e,s}} = 2.170$ h, which indicates that the initial jam propagation has caused a delay about 0.106 h and 0.109 h, respectively, as simply compared with the value of $T_{\mathrm{tav,s}}$.

For $\rho_0 = 0.666$, a value identical to ρ_{c2}, our numerical tests have predicted two travel time values, the first 5.488 h based on the present model, and the second 5.491 h based on the model of Zhang[44]. Since the second critical speed is assigned to be 15 km/h, the travel time with respect to the speed is 5.333 h, implying that the initial jams have caused a delay about 0.155 h and 0.158 h, respectively, slightly less than 10 min.

It is noted that the discrepancy from the model choice is rather small. The main reason is that the flow patterns based on the two models certainly are quite similar when the same traffic and sound curves as shown in Fig. 2 are employed. The travel time increases more rapidly when the ring road is more congested. For instance, when the initial density is 0.88 corresponding to $u_{\mathrm{e}}|_{\rho=0.88} = 0.018\,7 v_{\mathrm{f}}$, the travel time can be as more as about 40 h, but far smaller than that estimated from the equilibrium speed 53.48 h. This implies that for over second critical cases, the simply estimation approach of travel time with equilibrium is unavailable.

The travel time is primarily dependent on the road density ρ_0, indicating that to avoid the occurrence of those modes at over-second critical points, traffic control at the time to work or off work in urban regions is necessary. Many researchers treat the increase in the travelling time with an accidental drop of handling capacity of the road. The performed numerical simulations based on the dynamical model demonstrate that a sudden increase in the travelling time could be also the result of changing the flow mode for the same handling capacity. As shown in Fig. 1, there could exist two steady modes for one and the same capacity (two intersections of the fundamental curve with a horizontal line). The left intersection corresponds to a low traffic density and high travelling velocity. That yields a short travel time. The right intersection corresponds to a high density and low velocity, which gives the same capacity in terms of vehicles flux, but takes much longer time for each vehicle to reach destination.

The traffic flow mode evolution from one steady state to the other maintains the capacity, but drastically changes density, velocity, and, as a result, travel time. The effect of hysteresis, actually, is closely related to those changes in the traffic flow modes. Many external effects can cause changing of the steady-state equilibrium regime. The results of the present study demonstrate that the evolution of traffic flow between those regimes does not go symmetrically, as shown in Figs. 5–8. The change from low density to high density regimes is very fast, while restoring back the low density and high speed regime needs much more time.

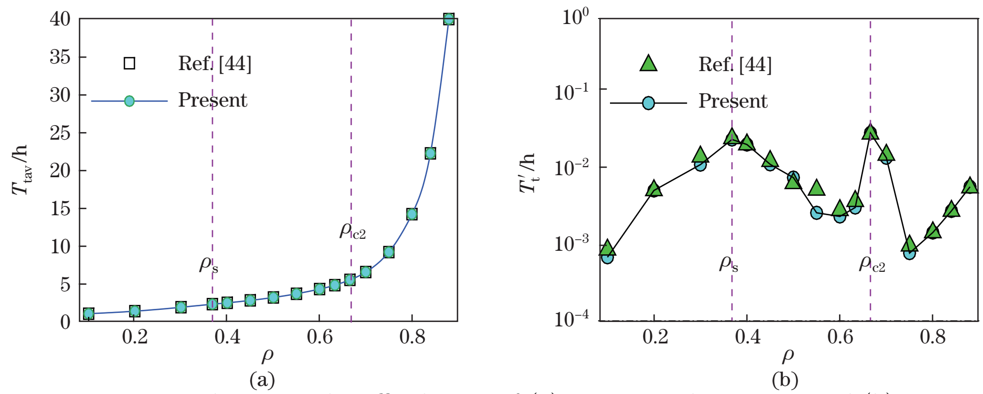

Fig. 12 Variations with ring road traffic density of (a) mean travel time $T_{\rm tav}$ and (b) its rms value $T_{\rm t}^{'}$

6 Conclusions

By predicting the travel time through a ring road with a VEM, where mathematical modeling of traffic pressure and sound speed is presented in the convenience of a suitable explanation of the specific traffic stoppage problem particularly discussed by Daganzo[60], several findings can be listed below.

(i) On using the VEM in numerical tests with a TVD scheme, it is found that for the traffic flow at saturation, spatial-temporal evolutions of traffic density reveal that several traffic jams between the initial jams can be spontaneously generated, and their colliding with the backward propagating initial jams can change the jams intensity and propagation direction. For congested traffic at the second critical, initial jams may occur cleavage.

(ii) The travel time predicted by the VEM is almost the same as that predicted by the model of Zhang[44]. For all traffic flows with initial density less than the second critical value, the ring road travel time can be simply estimated by the equilibrium speed decided by fundamental diagram. However, when the initial density is 0.88, the travel time can be as more as about 40 h, a value far smaller than that estimated by the equilibrium speed 53.48 h. This indicates that for over second critical cases, the simply estimation approach of travel time with equilibrium is unavailable.

(iii) The numerical results reveal that it is necessary to control traffic flows in congested scenarios, such as those might appear at the time to work or off work in urban regions.

References

[1] LIGHTHILL, M. J. and WHITHAM, G. B. On kinematic waves ii: a theory of traffic flow on long crowded roads. *Proc. Roy. Soc. Lond A*, **229**, 317–345 (1955)

[2] RICHARDS, P. I. Shock waves on the freeway. *Operations Res.*, **4**, 42–51 (1956)

[3] PAYNE, H. J. Models of freeway traffic and control. *Mathematical Model of Public Systems, Simulation Council Proc. La Jola California*, **1**, 51–61 (1971)

[4] HELBING, D. and TREIBER, M. Gas-kinetic-based traffic model explaining observed hysteretic phase transition. *Phys. Rev. Lett.*, **81**, 3042–3045 (1998)

[5] HOOGENDOORN, S. P. and BOVY, P. H. L. Continuum modeling of multiclass traffic flow. *Transp. Res. Part B*, **34**(2), 123–146 (2000)

[6] KERNER, B. S. and KONHÄUSER, P. Cluster effect in initially homogemeous traffic flow. *Phys. Rev. E*, **48**, 2335–2338 (1993)

[7] GREENBERG, J. M. Congestion redux. *SIAM J. Appl. Math.*, **64**(4), 1175–1185 (2004)

[8] BORSCHE, R., KIMATHI, M., and KLAR, A. A class of multi-phase traffic theories for microscopic, kinetic and continuum traffic models. *Computers and Mathematics with Applications*, **64**, 2939–2953 (2012)

[9] LEBACQUE, J. P., MAMMAR, S., and HAJ-SALEM, H. *Generic Second Order Traffic Flow Modelling. Transportation and Traffic Theory* (eds. ALLSOP, R. E. and BENJIAMIN, G. H.) Oxford, 755–776 (2007)

[10] LEBACQUE, J. P. and KHOSHYARAN, M. M. A variational formulation for higher order macroscopic traffic flow models of the gsom family. *Transp. Res. Part B*, **57**, 245–265 (2013)

[11] ZHANG, P., WONG, S. C., and DAI, S. Q. A conserved higher order aniso-tropic traffic flow model: description of equilibrium and non-equilibrium flows. *Transp. Res. Part B*, **43**(5), 562–574 (2009)

[12] FLYNN, M. R., KASIMOV, A. R., NAVE, J. C., ROSALES, R. R., and SEIBOLD, B. Self-sustained nonlinear waves in traffic flow. *Phys. Rev. E*, **79**, 056113 (2009)

[13] HELBING, D. Traffic and related self-driven many-particle systems. *Rev. Mod. Phys.*, **73**, 1067–1141 (2001)

[14] NAGATANI, T. The physics of traffic jams. *Rep. Prog. Phys.*, **65**, 1331–1386 (2002)

[15] BRACKSTONE, M. and MCDONALD, M. Car-following: a historical review. *Transp. Res. Part F*, **2**, 181–196 (1999)

[16] NAGEL, K. and SCHRECKENBERG, M. A cellular automaton model for freeway traffic. *J. De Phys. I*, **2**(12), 2221–2229 (1992)

[17] HELBING, D. and HUBERMAN, B. A. Coherent moving states in highway traffic. *nature*, **396** (6713), 738–740 (1998)

[18] CHOWDHURY, D., SANTEN, L., and SCHADSSCHNEIDER, A. Statistical physics of vehicular traffic and some related systems. *Physics Reports*, **329**, 199–329 (2000)

[19] NGODUY, D. Application of gas-kinetic theory to modelling mixed traffic of manual and adaptive cruise control vehicles. *Transportmetrica A*: *Transport Science*, **8**(1), 43–60 (2012)

[20] NGODUY, D. Platoon-based macroscopic model for intelligent traffic flow. *Transportmetrica B*: *Transport Dynamics*, **1**(2), 153–169 (2013)

[21] LI, J. and ZHANG, H. M. The variational formulation of a non-equilibrium traffic flow model: theory and implications. *Procedia-Social and Behavioral Sciences*, **80**, 327–340 (2013)

[22] ZHU, Z. J. and YANG, C. Visco-elastic traffic flow model. *J. Advanced Transp.*, **47**, 635–649 (2013)

[23] TORDEUX, A., ROUSSIGNOL, M., LEBACQUE, J. P., and LASSARRE, S. A stochastic jump process applied to traffic flow modelling. *Transportmetrica A*: *Transport Science*, **10**(4), 350–375 (2014)

[24] COSTESEQUE, G. and LEBACQUE, J. P. A variational formulation for higher order macroscopic traffic flow models: numerical investigation. *Transp. Res. Part B*, **70**, 112–133 (2014)

[25] BOGDANOVA, A. I., SMIRNOVA, M. N., ZHU, Z. J., and SMIRNOV, N. N. Exploring peculiarities of traffic flows with a viscoelastic model. *Transportmetrica A*: *Transport Science*, **11**(7), 561–578 (2015)

[26] SMIRNOVA, M. N., BOGDANOVA, A. I., ZHU, Z. J., and SMIRNOV, N. N. Traffic flow sensitivity to viscoelasticity. *Theoretical and Applied Mechanics Letters*, **6**, 182–185 (2016)

[27] SMIRNOVA, M. N., BOGDANOVA, A. I., ZHU, Z. J., and SMIRNOV, N. N. Traffic flow sensitivity to parameters in viscoelastic modelling. *Transportmetrica B*: *Transport Dynamics*, **5**(1), 115–131 (2017)

[28] ZHANG, Y. L., SMIRNOVA, M. N., BOGDANOVA, A. I., ZHU, Z. J., and SMIRNOV, N. N. Travel time estimation by urgent-gentle class traffic flow model. *Transp. Res. Part B*, **113**, 121–142 (2018)

[29] CHANG, G. L. and MAHMASSANI, H. S. Travel time prediction and departure time adjustment behavior dynamics in a congested traffic system. *Transp. Res. Part B*, **22**, 217–232 (1988)

[30] DAILEY, D. J. Travel-time estimation using cross-correlation techniques. *Transp. Res. Part B*, **27**(2), 97–107 (1993)

[31] LINT, J. V. and DER ZIJPP, N. V. Improving a travel-time estimation algorithm by using dual loop detectors. *Transp. Res. Rec.*, **1855**, 41–48 (2003)

[32] CHIEN, S. I. J. and KUCHIPUDI, C. M. Dynamic travel time prediction with real-time and historic data. *ASCE J. Transp. Eng.*, **129**(6), 608–616 (2003)

[33] WU, C. H., MO, J. M., and LEE, D. T. Travel-time prediction with support vector regression. *IEEE Trans. Intell. Transp. Syst.*, **5**(4), 276–281 (2004)

[34] VAN LINT, J. W. C., HOOGENDOORN, S. P., and VAN ZUYLEN, H. J. Accurate freeway travel time prediction with state-space neural networks under missing data. *Transp. Res. Part C*, **13**, 347–369 (2005)

[35] HOFLEITNER, A., HERRING, R., and BAYEN, A. Arterial travel time forecast with streaming data: a hybrid approach of flow modeling and machine learning. *Transp. Res. Part B*, **46**, 1097–1122 (2012)

[36] RAMEZANI, M. and GEROLIMINIS, N. On the estimation of arterial route travel time distribution with markov chains. *Transp. Res. Part B*, **46**, 1576–1590 (2012)

[37] JENELIUS, E. and KOUTSOPOULOS, H. N. Travel time estimation for urban road networks using low frequency probe vehicle data. *Transp. Res. Part B*, **53**, 64–81 (2013)

[38] YILDIRIMOGLU, M. and GEROLIMINIS, N. Experienced travel time prediction for congested freeways. *Transp. Res. Part B*, **53**, 45–63 (2013)

[39] HANS, E., CHIABAUT, N., and LECLERCQ, L. Applying variational theory to travel time estimation on urban arterials. *Transp. Res. Part B*, **78**, 169–181 (2015)

[40] KUMAR, B. A., VANAJAKSHI, L., and SUBRAMANIAN, S. C. Bus travel time prediction using a time-space discretization approach. *Transp. Res. Part C*, **79**, 308–332 (2017)

[41] CHANG, G. L. and MAHMASSANI, H. S. Travel time prediction and departure time adjustment behavior dynamics in a congested traffic system. *Transp. Res. Part B*, **22**, 217–232 (1988)

[42] MA, Z. L., KOUTSOPOULOS, H. N., FERREIRA, L., and MESBAH, M. Estimation of trip travel time distribution using a generalized markov chain approach. *Transp. Res. Part C*, **74**, 1–21 (2017)

[43] RAHMANI, M., KOUTSOPOULOS, H. N., and JENELIUS, E. Travel time estimation from sparse floating car data with consistent path inference: a fixed point approach. *Transp. Res. Part C*, **85**, 628–643 (2017)

[44] ZHANG, H. M. Driver memory, traffic viscosity and a viscous vehicular traffic flow model. *Transp. Res. Part B*, **37**, 27–41 (2003)

[45] DEL CALSTILLO, J. M. Propagation of perturbations in dense traffic flow: a model and its implications. *Transp. Res. Part B*, **35**, 367–389 (2001)

[46] HILLIGES, M. and WEIDLICH, W. A phenomenological model for dynamic traffic flow in networks. *Transp. Res. Part B*, **29**(6), 407–431 (1995)

[47] KERNER, B. S. Synchronized flow as a new traffic phase and related problems for traffic flow modelling. *Mathematical and Computer Modelling*, **35**, 481–508 (2002)

[48] SCHÖNHOF, M. and HELBING, D. Criticism of three-phase traffic theory. *Transp. Res. Part B*, **43**, 784–797 (2009)

[49] HAN, S. F. *Constitutive Theory of Viscoelastic Fluids* (in Chinese), Science Press, Beijing, 59–86 (2000)

[50] SMIRNOV, N. N., KISELEV, A. B., NIKITIN, V. F., SILNIKOV, V. F., and MANENKOVA, A. S. Hydrodynamic traffic flow models and its application to studying traffic control effectiveness. *WSEAS Transactions on Fluid Mechanics*, **9**, 178–186 (2014)

[51] SMIRNOV, N. N., KISELEV, A. B., NIKITIN, V. F., and YUMASHEV, M. V. Mathematical modelling of road traffic flows. *Moscow University Mechanics Bulletin*, **55**(4), 12–18 (2000)

[52] KISELEV, A. B., KOKOLEVA, A. V., NIKITIN, V. F., and SMIRNOV, N. N. Mathematical modeling of traffic flow on controled roads. *J. Appl. Math. Mech.*, **68**, 933–939 (2004)

[53] SMIRNOVA, M. N., BOGDANOVA, A. I., ZHU, Z. J., MANENKOVA, A. S., and SMIRNOV, N. N. Mathematical modeling of traffic flows using continuum approach: visco-elastic effect in traffic flows (in Russian). *Mathem. Mod.*, **26**, 54–64 (2014)

[54] AW, A. and RASCLE, M. Resurrection of second order models of traffic flow. *SIAM J. Appl. Math.*, **60**, 916–938 (2000)

[55] KLAR, A. and WEGENER, R. Kinetic derivation of macroscopic anticipation models for vehicular traffic. *SIAM J. Appl. Math.*, **60**, 1749–1766 (2000)

[56] KISELEV, A. B., NIKITIN, V. F., SMIRNOV, N. N., and YUMASHEV, M. V. Irregular traffic flow on a ring road. *J. Appl. Math. Mech.*, **64**(4), 627–634 (2000)

[57] ZHU, Z. J., WU, Q. S., JIANG, R., and WU, T. Q. Numerical study on traffic flow with single parameter state equation. *ASCE J. Transp. Engineering*, **128**, 167–172 (2002)

[58] HAIGHT, F. A. *Mathematical Theories of Traffic Flow*, Academic Press, New York, 89–92 (1963)

[59] MA. J., CHAN, C. K., YE, Z. B., and ZHU, Z. J. Effects of maximum relaxation in viscoelastic traffic flow modeling. *Transp. Res. Part B*, **113**, 143–163 (2018)

[60] DAGANZO, C. F. Requiem for second-order fluid approximations of traffic flow. *Transp. Res. Part B*, **29**, 277–286 (1995)

[61] RASCLE, M. An improved macroscopic model of traffic flow: derivation and links with the lighthill-whitham model. *Mathematical and Computer Modelling*, **35**, 581–590 (2002)

[62] XU, R. Y., ZHANG, P., DAI, S. C., and WONG, S. C. Admissibility of a wide cluster solution inanisotropic higher-order traffic flow models. *SIAM J. Appl. Math.*, **68**(2), 562–573 (2007)

[63] ROE, P. C. Approximate riemann solver, parameter vectors, and difference schemes. *J. Comput. Phys.*, **43**, 357–372 (1981)

[64] SHUI, H. S. *Finite Difference in One-dimensional Fluid Mechanics* (in Chinese), National Defense, Beijing, 333–355 (1998)

[65] ZHU, Z. J. and WU, T. Q. Two-phase fluids model for freeway traffic and its application to simulate the evolution of solitons in traffic. *ASCE J. Transp. Engineering*, **129**, 51–56 (2003)

[66] CHANG, G. L. and ZHU, Z. J. A macroscopic traffic model for highway work zones: formulations and numerical results. *J. Advanced Transp.*, **40**(3), 265–287 (2006)

[67] TAO, W. Q. *Numerical Heat Transfer* (in Chinese), Xian Jiaotong University Press, Xi'an, 195–251 (2001)

[68] DAGANZO, C. F. *Fundamentals of Transportation and Traffic Operations*, Pergamon, New York, 110–112 (1997)

[69] MCSHANE, W. R., ROESS, R. P., and PRASSAS, E. S. *Traffic Engineering*, Chap. 12, 2nd ed., Prentice-Hall, New Jersey, 282–306 (1998)

[70] DRAKE, J. S., SCHOFER, J. L., and MAY, A. D., JR. A statistical analysis of speed-density hypothesis. *Transportation Research Record*, **154**, 81–82 (1967)